Supplementary Information

for

Device Deficiency and Degradation Diagnosis Model of Perovskite Solar Cells through Hysteresis Analysis

Zi Shuai Wang[1,8], Yidan An[2,8], Xingang Ren[3,8], Hong Zhang[4,8], Zhenfeng Huang[1], Hin-Lap Yip[2,5,6], Zhixiang Huang[3], Wallace C.H. Choy[1,7,*]

[1] Department of Electrical and Electronic Engineering, The University of Hong Kong, Pok Fu Lam Road, Hong Kong SAR, China.

[2] Department of Materials Science and Engineering, City University of Hong Kong, Kowloon, Hong Kong 999077, China.

[3] Information Materials and Intelligent Sensing Laboratory of Anhui Province, Institute of Physical Science and Information Technology, Anhui University, Hefei, 230601, China.

[4] State Key Laboratory of Photovoltaic Science and Technology, Shanghai Frontiers Science Research Base of Intelligent Optoelectronics and Perception, Institute of Optoelectronics, Fudan University, Shanghai 200433, China.

[5] School of Energy and Environment, City University of Hong Kong, Kowloon, Hong Kong 999077, China.

[6] Hong Kong Institute for Clean Energy, City University of Hong Kong, Kowloon, Hong Kong 999077.

[7] Materials Innovation Institute for Life Sciences and Energy (MILES), HKU-SIRI, Shenzhen, P.R. China.

[8] These authors contributed equally: Zi Shuai Wang, Yidan An, Xingang Ren, Hong Zhang.

[*] E-mail: chchoy@eee.hku.hk

Supplementary Note 1: The model of hysteresis effect of perovskite solar cells (PSCs)

1.1 Governing Equations of ion-incorporated drift-diffusion model

The governing equations of the ion-incorporated drift-diffusion model are listed as below [1-4]. Eqs.1-4 represent the continuity equations of electron, hole, anion and cation mobile ionic carrier, where J_n, J_p, J_a and J_c are the current of electron, hole, anion and cation ionic carrier respectively; G and R denote the free carrier generation rate and recombination rate of electron and hole, respectively. Eq. 5 is Poisson's equation, considering doping (N_A, N_D), anion and cation mobile ionic carrier (a, c). ε_0 and ε_r are the vacuum dielectric constant and the relative dielectric constant. Generation rate G can be uniform in the absorber for simplification, or depth-dependent, imported from optical simulation[5]. R in the modeling includes the intrinsic radiative (band to band) and defect-assisted Shockley-Read-Hall (SRH) recombination terms, whereas Auger recombination can be ignored in PSCs[6]. There is no generation nor recombination terms for mobile ions, as the total amount of mobile ions are fixed. The recombination kinetic equations are shown in Eqs. 6-7[7,8].

$$\frac{\partial n}{\partial t} = \frac{1}{q}\frac{\partial J_n}{\partial x} + G - R \tag{1}$$

$$\frac{\partial p}{\partial t} = -\frac{1}{q}\frac{\partial J_p}{\partial x} + G - R \tag{2}$$

$$\frac{\partial a}{\partial t} = \frac{1}{q}\frac{\partial J_a}{\partial x} \tag{3}$$

$$\frac{\partial c}{\partial t} = -\frac{1}{q}\frac{\partial J_c}{\partial x} \tag{4}$$

$$\frac{\partial}{\partial x}\left(\varepsilon_0 \varepsilon_r \frac{\partial V}{\partial x}\right) = -q(p - n + c - a + N_A - N_D) \tag{5}$$

$$R_{rad} = k_{rad}(np - n_i^2) \tag{6}$$

$$R_{SRH} = \frac{np - n_i^2}{\tau_n(p + p_t) + \tau_p(n + n_t)} \tag{7}$$

where n_i refers to the intrinsic carrier density which is determined by the bandgap and temperature. Capture coefficient and density of the defect are represented by the reciprocal of their product, SRH lifetime $\tau_{n(p)}$, which is intuitional and directly related to the characteristic lifetime measured in transient photoluminescence study. Trapped electron and hole densities are n_t and p_t, respectively, which depend on the energy levels of their trap states. The drift-diffusion equations of electron, hole, cation and anion mobile ion are shown in Eqs. 8-11:

$$J_n = q\mu_n\left(-n\frac{d\psi_n}{dx} + k_B T\frac{dn}{dx}\right) \tag{8}$$

$$J_p = q\mu_p\left(-p\frac{d\psi_p}{dx} - k_B T\frac{dp}{dx}\right) \quad (9)$$

$$J_a = q\mu_a(-a\frac{dV}{dx} + k_B T\frac{da}{dx}) \quad (10)$$

$$J_c = q\mu_c(-c\frac{dV}{dx} - k_B T\frac{dc}{dx}) \quad (11)$$

Carrier mobilities of electron, hole, and positive mobile ionic carrier are μ_n, μ_p, μ_a, respectively. T refers to device temperature, and k_B is the Boltzmann constant. It is worth noting that the potential terms in Eqs. 8-9, $\psi_{n/p}$, and in Ep. 10-11, V, are different, as $\psi_{n/p}$ includes the influence from the energy band structures:

$$\psi_n = V + \frac{\chi}{q} + \frac{k_B T}{q}\ln(N_c) \quad (12)$$

$$\psi_p = V + \frac{\chi}{q} + \frac{E_g}{q} - \frac{k_B T}{q}\ln(N_V) \quad (13)$$

where V is just the electrical potential term as in Eq. 5. Moreover, χ is electron affinity, E_g is bandgap, and $N_{C/V}$ is the effective density of state of conduction band or valence band. Eqs. 12-13 take into account the driving force from energy band bending, e.g. heterojunction, and thus enable the simulation of carrier extraction and injection at the interfaces in multi-layer device architecture.

Four continuity equations of electron and hole, current boundary conditions were applied, as:

$$J_{nc} = S_{nc}(n - n_{0c}) \quad (14)$$

$$J_{na} = S_{na}(n - n_{0a}) \quad (15)$$

$$J_{pc} = S_{pc}(p - p_{0c}) \quad (16)$$

$$J_{pa} = S_{pa}(p - p_{0a}) \quad (17)$$

where S_{nc}, S_{pa}, S_{na}, S_{pc} are surface recombination velocities applied for electrodes, and n_{0c}, n_{0a}, p_{0c}, p_{0a} are the boundary values of electron and hole densities at the cathode (subscript c) and anode (subscript a) electrodes, respectively, determined by the Schottky barriers. It should be noted that infinite large surface recombination velocities for majority carriers (S_{nc}, S_{pa}) and zero surface recombination velocities for minority carriers (S_{np}, S_{pc}) represent the case of perfectly selective electrodes.

Although the penetration of ions into carrier transporting layers (CTLs) or even electrodes are reported[9-11], it is still questionable whether the ions that penetrated in CTLs can move freely and back to perovskite, then affect the device performance electrically like in the perovskite bulk. In this work, to model the more general problems, we assume the mobile ions will only move in the perovskite bulk region, and the interfaces between

perovskite and CTLs will block their transport. For the continuity equation of positive mobile ion, Dirichlet boundary condition was applied at the two sides:

$$a(x = 0) = a(x = d) = 0 \quad (18)$$

where $x=0$ and $x=d$ represent the positions of cathode and anode, respectively, and d refers to the device thickness. The zero mobility is set for the mobile ion in CTL regions including both electron transporting layer (ETL) and hole transporting layer (HTL). This setting is equivalent to the $J_a=0$ boundary conditions at the interfaces between perovskite and CTLs.

For Poisson's equation, we applied the Dirichlet boundary condition:

$$V(x = 0) = -WF_{cathode} \quad (19)$$

$$V(x = d) = V_{app} - WF_{anode} \quad (20)$$

where $WF_{cathode/anode}$ is the work function of cathode or anode, and V_{app} is the externally applied voltage. The Scharfetter-Gummel based finite-difference discretization form of the governing equations in space and time domain are described in next section. The computation procedure is schematically expressed in **Scheme 1**:

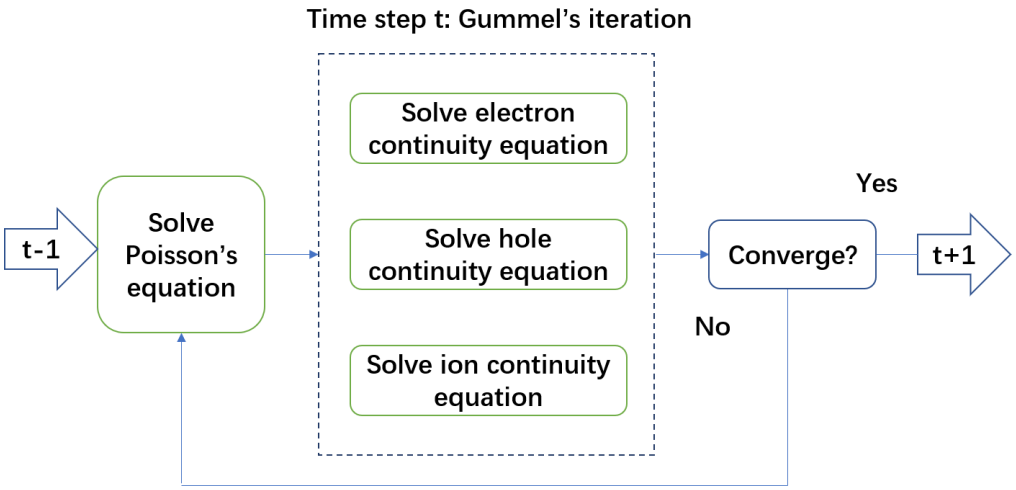

Supplementary Figure 1. The flowchart of the transient ion-incorporated drift-diffusion simulation.

Compared to the existing programs, this simulation method does not rely on any of the commercial software or commercial PDE solver toolbox, and can be easily realized in the popular programming platforms like Python, MATLAB or C++ [12].

The input parameters (**Supplementary Tables 1**) and the n-i-p multi-layer simulation device structure (**Supplementary Tables 2**) used for the simulation are given in next section. It should be noted that we consider the following assumptions in this work:

i) mobile ionic carriers can move in the perovskite bulk region, but should be insulated by the perovskite/CTL interfaces, in which the ions penetrated into CTLs are not considered;

ii) mobile ion should not react directly with electron or hole, like collision or mobile-ion induced recombination;

iii) ion distribution evolution with time can naturally influence the device by changing the E-field.

These assumptions should be valid for most of the reported PSCs, but might be invalid for some of the devices with fullerene-based CTLs, in which the effect of ion accumulation at the fullerene surface is still questionable[13,14].

1.2 Discretization form of the governing equations and the explanations

The discretization form of the governing equations in space and time domain are expressed in Eqs. 20-23 which are most important to ensure the stable computation. Drift-diffusion terms were discretized by Scharfetter-Gummel scheme in space domain[4], and by modified backward Euler method in time domain. $B(x)$ refer to the Bernoulli function.

$$\left[-2\times\frac{\varepsilon_{i+\frac{1}{2}}+\varepsilon_{i-\frac{1}{2}}}{2\Delta x^2}-\frac{n_i^j+p_i^j}{k_BT}\right]V_i^j+\varepsilon_{i+\frac{1}{2}}\frac{V_{i+1}^j}{\Delta x^2}+\varepsilon_{i-\frac{1}{2}}\frac{V_{i-1}^j}{\Delta x^2}=-q\left(-n_i^j+p_i^j+N_D-N_A\right)-\frac{V_i^{j-1}\left(n_i^j+p_i^j\right)}{k_BT} \quad (20)$$

$$\left[\frac{1}{\Delta t}+\frac{D_{n_{i+1/2}}}{\Delta x^2}B\left(\frac{\psi_{n,i}-\psi_{n,i+1}}{k_BT}\right)+\frac{D_{n_{i-1/2}}}{\Delta x^2}B\left(\frac{\psi_{n,i}-\psi_{n,i-1}}{k_BT}\right)+k_{rad}p_i^{j-1}+\frac{p_i^{j-1}}{\tau_n\left(p_i^{j-1}+p_t\right)+\tau_p(n_i^{j-1}+n_t)}\right]n_i^j-\left[\frac{D_{n_{i+1/2}}}{\Delta x^2}B\left(\frac{\psi_{n,i+1}-\psi_{n,i}}{k_BT}\right)\right]n_{i+1}^j-\left[\frac{D_{n_{i-1/2}}}{\Delta x^2}B\left(\frac{\psi_{n,i-1}-\psi_{n,i}}{k_BT}\right)\right]n_{i-1}^j=\frac{n_i^{j-1}}{\Delta t}+G_i-\frac{n_{in}^2}{\tau_n\left(p_i^{j-1}+p_t\right)+\tau_p(n_i^{j-1}+n_t)}-k_{rad}n_{in}^2 \quad (21)$$

$$\left[\frac{1}{\Delta t}+\frac{D_{p_{i+\frac{1}{2}}}}{\Delta x^2}B\left(-\frac{\psi_{p,i}-\psi_{p,i+1}}{k_BT}\right)+\frac{D_{p_{i-\frac{1}{2}}}}{\Delta x^2}B\left(-\frac{\psi_{p,i}-\psi_{p,i-1}}{k_BT}\right)+k_{rad}n_i^{j-1}+\frac{n_i^{j-1}}{\tau_n\left(p_i^{j-1}+p_t\right)+\tau_p\left(n_i^{j-1}+n_t\right)}\right]p_i^j-\left[\frac{D_{p_{i+\frac{1}{2}}}}{\Delta x^2}B\left(-\frac{\psi_{p,i+1}-\psi_{p,i}}{k_BT}\right)\right]p_{i+1}^j-\left[\frac{D_{p_{i-\frac{1}{2}}}}{\Delta x^2}B\left(-\frac{\psi_{p,i-1}-\psi_{p,i}}{k_BT}\right)\right]p_{i-1}^j=\frac{p_i^{j-1}}{\Delta t}+G_i-\frac{n_{in}^2}{\tau_n\left(p_i^{j-1}+p_t\right)+\tau_p\left(n_i^{j-1}+n_t\right)}-k_{rad}n_{in}^2 \quad (22)$$

$$\left[\frac{1}{\Delta t}+\frac{D_{a_{i+\frac{1}{2}}}}{\Delta x^2}B\left(-\frac{V_i-V_{i+1}}{k_BT}\right)+\frac{D_{a_{i-\frac{1}{2}}}}{\Delta x^2}B\left(-\frac{V_i-V_{i-1}}{k_BT}\right)\right]a_i^j-\left[\frac{D_{a_{i+\frac{1}{2}}}}{\Delta x^2}B\left(-\frac{V_{i+1}-V_i}{k_BT}\right)\right]a_{i+1}^j-\left[\frac{D_{a_{i-\frac{1}{2}}}}{\Delta x^2}B\left(-\frac{V_{i-1}-V_i}{k_BT}\right)\right]a_{i-1}^j=\frac{a_i^{j-1}}{\Delta t} \quad (23)$$

where the subscript i and superscript j refer to the space and time domain grids. Δx and Δt are the space and time discretization steps, respectively. $D_{n,p,a}$ is the diffusion coefficient of electron, or hole, or positive mobile ion. It is worthy noting that the radiative and SRH recombination terms in Eqs. S2-S3 were split into two parts, which belong to two near time steps. Physically, it means the electron (or hole) at the current time step will

recombine with the hole (or electron) of the last time step. This method is applied to improve the stability of the computation, and will not influence the result as long as the evolution of carrier density is not so fast. These discretized form of equations can be solved using multifrontal sparse matrix inversion method[4] times by times in Gummel's iteration, until achieving the condition of convergence.

1.3 Surface recombination

$$R_{surf} = \frac{n^+ p^- - n_i^2}{\tau_{surfn}(p^- + p_t) + \tau_{surfp}(n^+ + n_t)} \tag{24}$$

The surface recombination at the interfaces between perovskite and CTLs is modeled by Eq. 24, and set at the two interfaces in the discussion about surface recombination. n^+ and p^- are the electron and hole densities on the two sides of the interface, respectively, and $\tau_{surfn(p)}$ donates the surface recombination lifetime, which is physically related to the reciprocal of the product of surface defect density and its capture cross section. However, this surface recombination lifetime is not expected to match any of the characteristic carrier lifetime measurement result, as the rate of the surface recombination also depends on the energy band offset between perovskite and the CTLs. Therefore, in this study, the energy band offset is fixed. The surface recombination term is coupled in the drift-diffusion model by the same methods as bulk SRH recombination term.

1.4 Optoelectronic model of PSCs with obtaining hysteresis effect

The optoelectronic model of PSCs with obtaining hysteresis effect was built by addressing a couple of carrier transport and Poisson's equations (equations 1-4). To obtain the carrier generation, the Maxwell's equations was also coupled solved with Equations 1-4. Thus, the model can obtain the optical information, including the optical absorption of devices and electromagnetic field distribution. Electrically, it can be used for analyzing the carrier transportation/recombination dynamics, energy band alignment, and the built-in potential/filed.

Supplementary Figures:

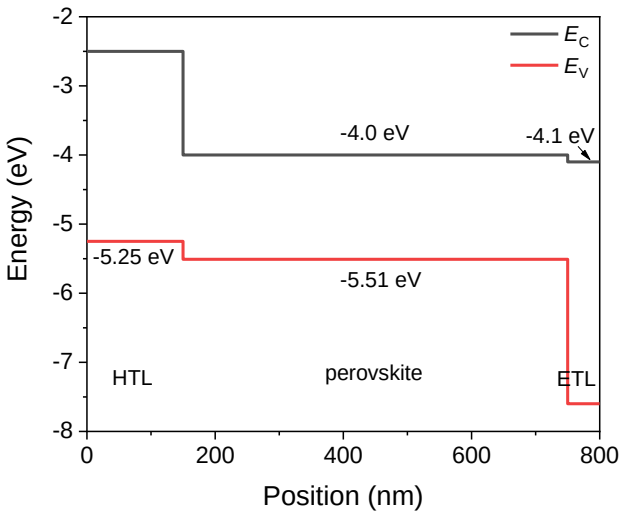

Supplementary Figure 2. Band diagram of the modeling device: ETL/Perovskite/HTL, where HTL is set as baseline and incident light from ETL side.

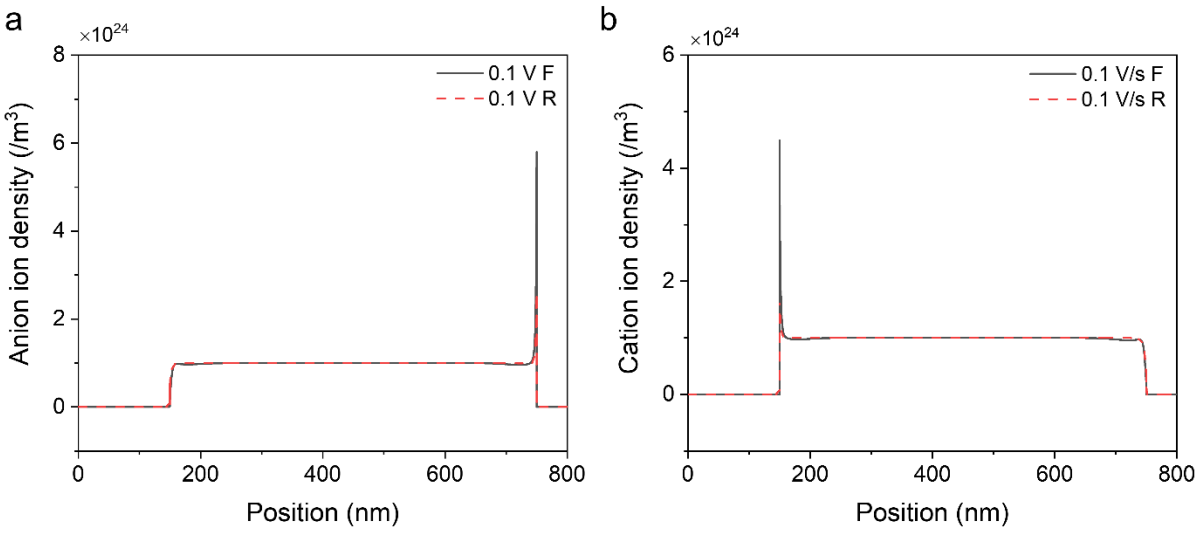

Supplementary Figure 3. a,b the anion and cation mobile ion distribution under the forward and reverse bias (0.8 V) with a scan rate of 0.1V/s, respectively.

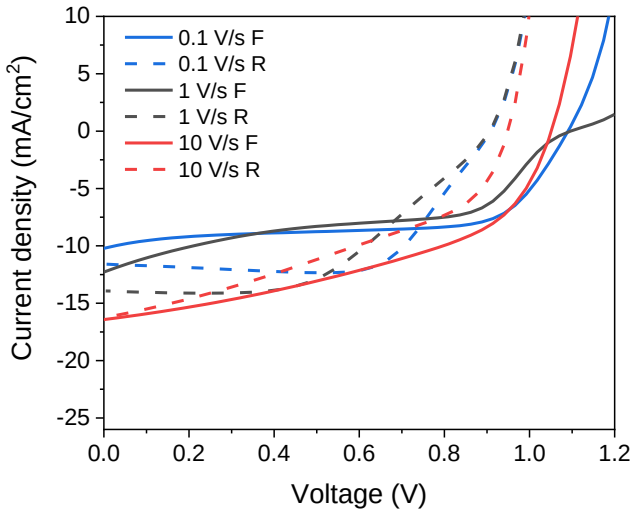

Supplementary Figure 4. Simulated hysteresis originated from dominated SRH recombination in perovskite bulk with τ_{SRH} = 10 ns and low carrier mobility μ = 0.2 cm^2/Vs

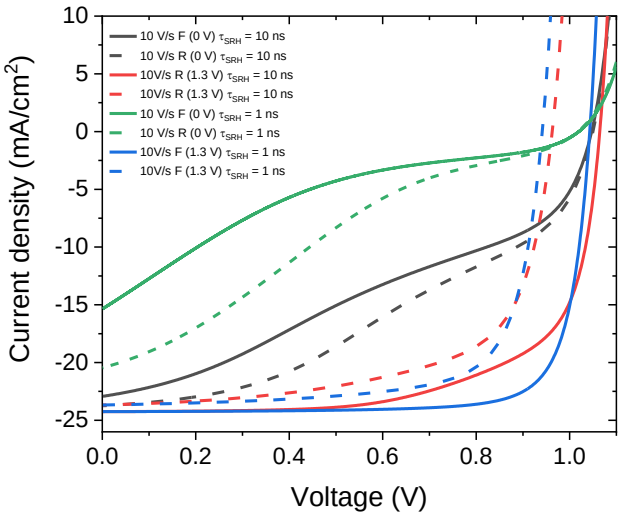

Supplementary Figure 5. Simulated hysteresis originated from dominated SRH recombination in perovskite bulk with τ_{SRH} = 1 ns and 10 ns, and FR and RF scan protocols. Orange lines are the same curves shown in **Fig. 3a** in the main text.

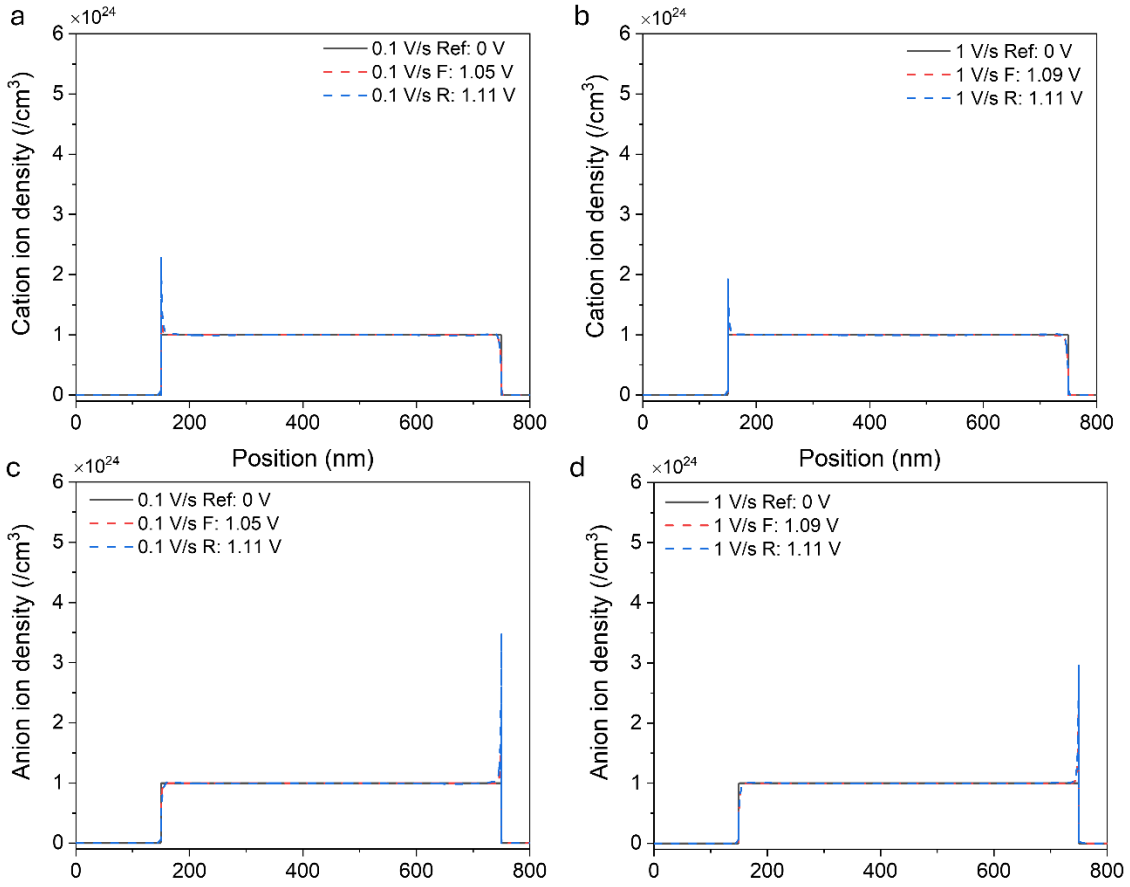

Supplementary Figure 6. Cation and anion ion density distributions at V_{oc} voltages of the modeling device in Figure. 4**c,d** with **a,c** 0.1 V/s and **b,d** 1 V/s rate.

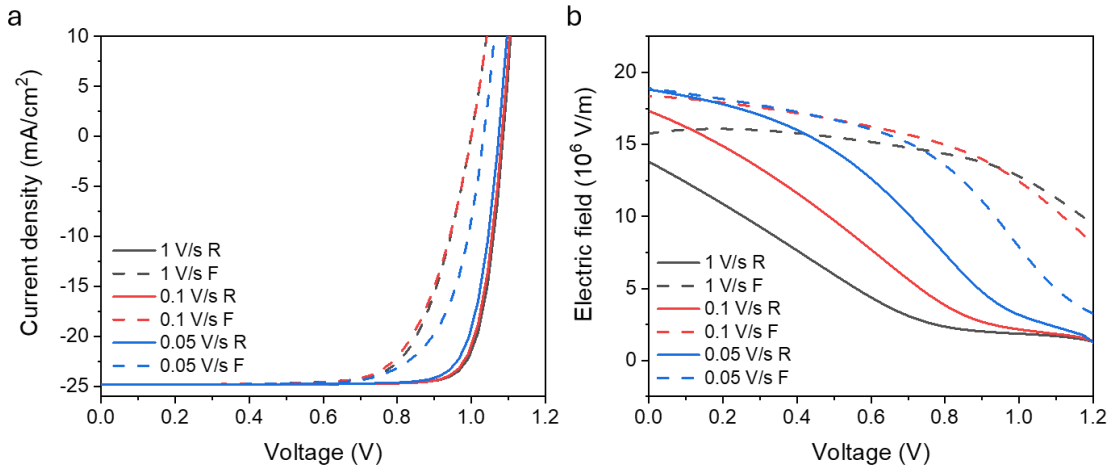

Supplementary Figure 7. a simulated hysteresis originated from dominated surface recombination at the interfaces between perovskite and CTLs with τ_{surf} = 10 ns and RF scan protocol. **b** simulated electric field at perovskite/HTL interface vs applied voltage with RF scan protocol.

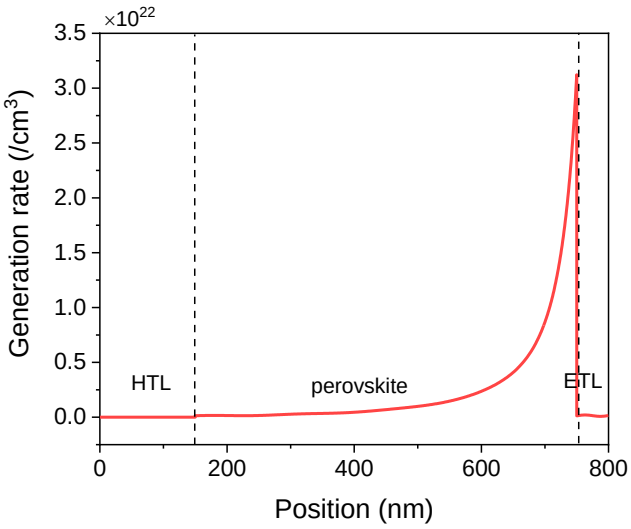

Supplementary Figure 8. Generation rate distribution inside the perovskite bulk region of the normal PSCs with structure (TiO_2/perovskite/ Spiro-OMeTAD/Au), where the HTL as the baseline and incident sunlight from ETL side. Realistic refractive indices were used.

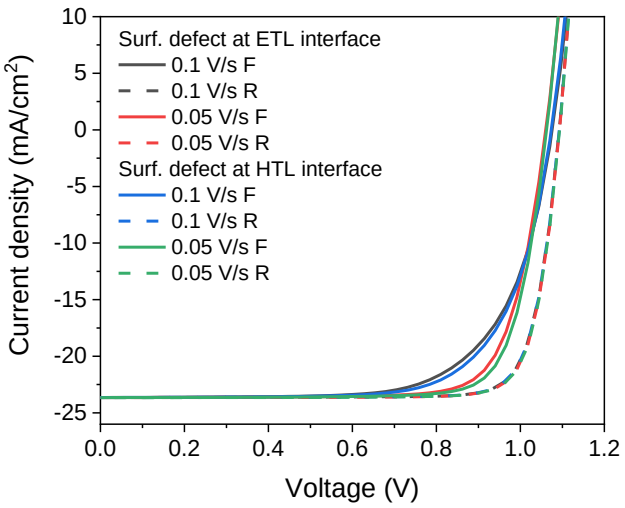

Supplementary Figure 9. Simulated hysteresis originated from dominated surface recombination at the interface between perovskite and ETL or HTL with τ_{surf} = 0.01 ns in normal-structure PSCs.

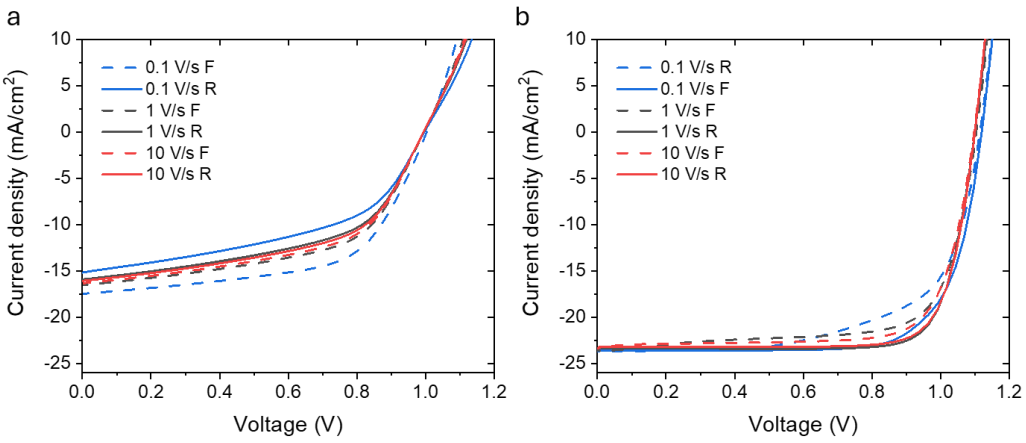

Supplementary Figure 10. a simulated hysteresis originated from bulk recombination τ_{SRH} = 1 ns and low electron mobility in ETL $\mu_n = 2\times10^{-5}$ cm^2/Vs with FR scan protocol. **b** bulk recombination τ_{SRH} = 10 ns and low electron mobility in ETL $\mu_n = 2\times10^{-4}$ cm^2/Vs with RF scan protocol.

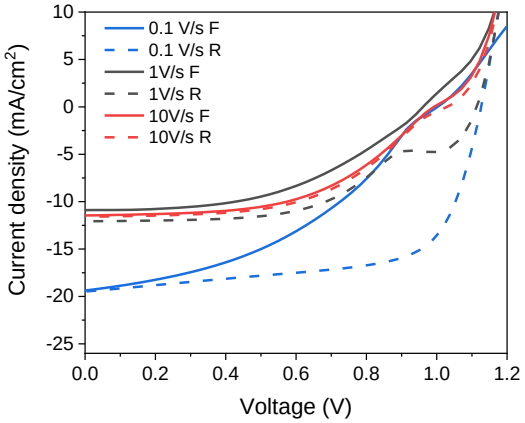

Supplementary Figure 11. Simulated hysteresis originated from surface recombination and low carrier mobility in perovskite with τ_{surf} = 1 ns, and μ = 0.02 cm^2/Vs. The major difference compared to **Supplementary Figure** 4 is the changing of V_{oc}.

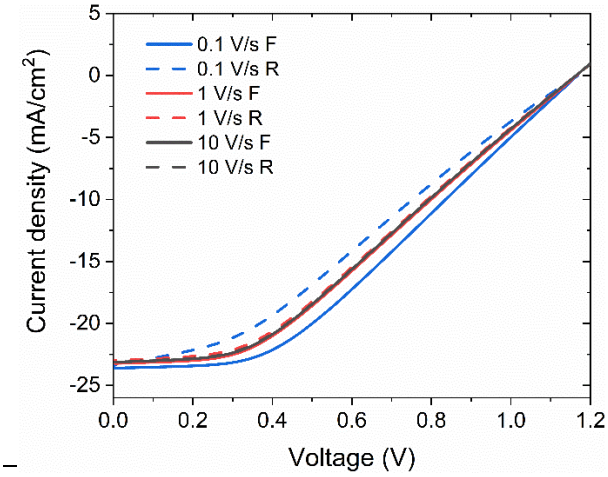

Supplementary Figure 12. Simulated hysteresis originated from surf recombination τ_{surf} = 1 ns and low electron mobility in ETL $\mu_n = 2\times10^{-5}$ cm^2/Vs with RF scan protocol.

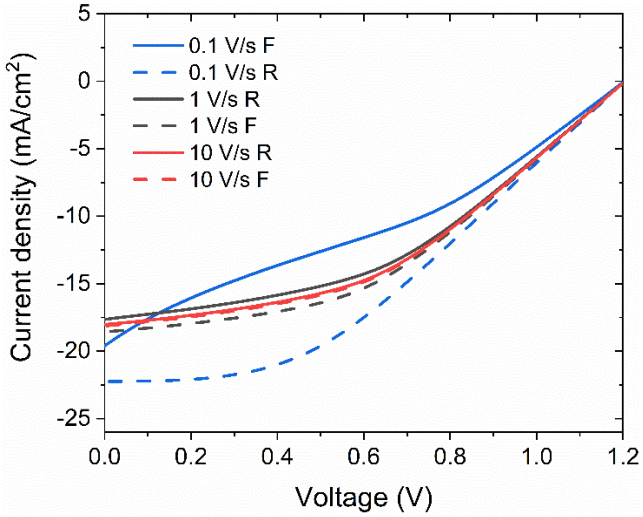

Supplementary Figure 13. Simulated hysteresis originated from low carrier mobility in ETL μ_n = 2×10^{-5} cm^2/Vs and in perovskite μ = 0.02 cm^2/Vs.

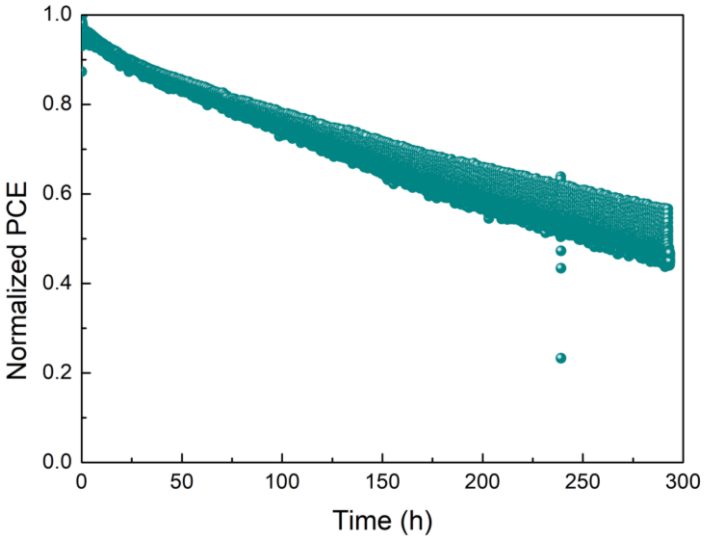

Supplementary Figure 14. The PCE of the unencapsulated PSCs measured at maximum power point under continuous one-sun illumination at 45 ± 5 °C in N_2 atmosphere.

Supplementary Tables: input parameters

Supplementary Tables 1. Input parameters used in the simulation in the paper

Parameter Names	Symbols [units]	Values		
		ETL	**Absorber**	**HTL**
Thickness	L [nm]	50	600	150
Bandgap	E_g [eV]	3.5	1.51	2.5
Electron affinity	χ [eV]	4.1	4.0	2.75
Effective Fermi level	E_0 [eV]	4.2	4.6	5.0
SRH lifetime for electron and hole	τ_{SRH} [μs]	1	1 (as default)	1
Nominal Radiative recombination coefficient	k_{rad} [cm^3/s]	$1.5*10^{-10}$	$3.6*10^{-12}$	$1.5*10^{-10}$
Electron mobility	μ_n [cm^2/Vs]	20 (as default)	20 [15] (as default)	0
Hole mobility	μ_p [cm^2/Vs]	0	20 [15] (as default)	20
Cation mobility	μ_a [cm^2/Vs]	0	10^{-10}	0
Initial cation density	a/c [$/cm^3$]	0	10^{18} [16]	0
Generation rate	G [$/m^3s$]	0	3×10^{27}	0
Density of state	$N_{c/v}$ [$/cm^3$]	10^{19}	10^{19}	10^{19}
Relative dielectric constant	ε_r	4	31 [17]	4
Schottky barrier	B_n, B_p [eV]	0.1	--	0.1

Supplementary Tables 2. Input parameters for the simulations in Figures 7, 8. The parameters not listed are the same as those in Table S1.

Parameter Names		**Symbols [units]**		**Values**		
				ETL	**Absorber**	**HTL**
Bandgap		E_g [eV]	Fig. 7	2.1	1.4	2.1
			Fig. 8	2.3	1.53	2.3
Electron affinity		χ [eV]	Fig. 7	4.1	3.8	2.8
			Fig. 8	4.1		2.8
Effective Fermi level		E_0 [eV]	Fig. 7	4.2	4.6	4.8
			Fig. 8	4.2		5.0
SRH lifetime for electron and hole		τ_{SRH}	Fig. 7	--	1 µs	--
			Fig. 8		10 ns to 0.5 ns	
Surface recombination		τ_{surf}	Fig. 7	--	3 ns to 10 ns	--
			Fig. 8		100 ns	

Supplementary References

1 Snaith, H. J. *et al.* Anomalous hysteresis in perovskite solar cells. *The Journal of Physical Chemistry Letters* **5**, 1511-1515 (2014).

2 Bertoluzzi, L. *et al.* Mobile ion concentration measurement and open-access band diagram simulation platform for halide perovskite solar cells. *Joule* **4**, 109-127 (2020).

3 Courtier, N. E., Richardson, G. & Foster, J. M. A fast and robust numerical scheme for solving models of charge carrier transport and ion vacancy motion in perovskite solar cells. *Appl. Math. Modell.* **63**, 329-348 (2018).

4 Selberherr, S. *Analysis and simulation of semiconductor devices*. (Springer-Verlag Wien, 1984).

5 Sha, W. E. I., Choy, W. C. H., Wu, Y. & Chew, W. C. Optical and electrical study of organic solar cells with a 2d grating anode. *Opt. Express* **20**, 2572-2580 (2012).

6 Lopez-Varo, P. *et al.* Device physics of hybrid perovskite solar cells: Theory and experiment. *Advanced Energy Materials* **8**, 1702772 (2018).

7 Ai, Z. *et al.* Physics, simulation, and experiment of perovskite solar cells with addressing hysteresis effect. *Sol. RRL* **6** (2022).

8 Lopez-Varo, P. *et al.* Device physics of hybrid perovskite solar cells: Theory and experiment. *Adv. Energy Mater.* **8** (2018).

9 Fakharuddin, A., Schmidt-Mende, L., Garcia-Belmonte, G., Jose, R. & Mora-Sero, I. Interfaces in perovskite solar cells. *Advanced Energy Materials* **7**, 1700623 (2017).

10 Jeangros, Q. *et al.* In situ tem analysis of organic–inorganic metal-halide perovskite solar cells under electrical bias. *Nano Letters* **16**, 7013-7018 (2016).

11 Zhang, T., Hu, C. & Yang, S. Ion migration: A "double-edged sword" for halide-perovskite-based electronic devices. *Small Methods* **4**, 1900552 (2020).

12 https://github.com/barnesgroupICL/Driftfusion. Https://github.Com/barnesgroupicl/driftfusion.

13 Chen, B., Yang, M., Priya, S. & Zhu, K. Origin of j–v hysteresis in perovskite solar cells. *The Journal of Physical Chemistry Letters* **7**, 905-917 (2016).

14 Garcia-Belmonte, G. & Bisquert, J. Distinction between capacitive and noncapacitive hysteretic currents in operation and degradation of perovskite solar cells. *ACS Energy Letters* **1**, 683-688 (2016).

15 Herz, L. M. Charge-carrier mobilities in metal halide perovskites: Fundamental mechanisms and limits. *ACS Energy Letters* **2**, 1539-1548 (2017).

16 Walsh, A., Scanlon, D. O., Chen, S., Gong, X. G. & Wei, S.-H. Self-regulation mechanism for charged point defects in hybrid halide perovskites. *Angewandte Chemie International Edition* **54**, 1791-1794 (2015).

17 Sendner, M. *et al.* Optical phonons in methylammonium lead halide perovskites and implications for charge transport. *Materials Horizons* **3**, 613-620 (2016).